A New View of the LHB and $\frac{1}{4}$ keV X-ray Halo

S.L. Snowden

NASA Goddard Space Flight Center, Code 662, Greenbelt, MD 20771, USA

Abstract. The X-ray sky at $\frac{1}{4}$ keV is completely dominated by diffuse emission. It has become clear that it originates as at least three separate components: local emission within the nearest ~ 100 pc from the Sun, halo emission from beyond most of the neutral material of the Galactic disk, and the superposition of unresolved extragalactic sources. The only way to determine the temperatures and relative emission measures of the hot plasma responsible for the Galactic components is to use the X-ray intensity variations due to column density variations in the intervening H I to separate the components. "Shadowing" studies have been pursued for individual objects using *ROSAT* data from both pointed observations and the all-sky survey with considerable success.

This paper presents the results of an all-sky analysis of the $\frac{1}{4}$ keV background from the *ROSAT* survey. A Local Hot Bubble is found consistent with, although somewhat smaller than, previous models. It has a temperature of $10^{6.1}$ K and an emission measure which varies by a factor of ~ 3.3 over large angles. The halo emission has a temperature near $10^{6.0}$ K with an emission measure which varies from near zero to more than five times that of the local emission.

1 Introduction

The source of the $\frac{1}{4}$ keV soft X-ray diffuse background (SXRB) has proved elusive since its discovery in the late 1960s (e.g., Bowyer, Field, & Mack 1968). The general negative correlation between the SXRB and the column density of Galactic neutral hydrogen (dominated by a Galactic plane-to-pole variation) was strongly suggestive of an "absorption" model, where the angular structure of the SXRB is produced by the absorption of a flux of distant origin (e.g., Marshall & Clark 1984). The absence of the expected detailed negative correlation (some specific H I features showed little indication of shadowing, e.g., Burrows et al. 1984), the shallowness of the apparent absorption, and the weakness of the energy dependence of the apparent absorption encouraged the investigation of other possibilities.

By the end of the 1980s, the displacement model (e.g., Sanders et al. 1977; Snowden et al. 1990, hereafter SCMS) proved to be the most consistent with the available data. The displacement model suggests that the irregularly shaped cavity which surrounds the Sun (known independently from interstellar absorption line studies: e.g., Frisch & York 1983, and $N_{\rm H}$ studies: e.g., Knapp 1975) contains an X-ray-emitting plasma, and that the cavity is extended more toward the Galactic poles than within the Galactic

plane. The greater the extent of the plasma-filled cavity in a given direction, the greater the emission measure of the plasma and the lower the measured column density of H I (at constant Galactic latitudes), which produces the general negative correlation between the two. The displacement model provided a natural explanation for the weakness and energy independence of the apparent absorption and allowed for H I features which had no apparent effect on the X-ray flux.

With the launch of the *Röntgensatellit* (*ROSAT*, Trümper 1983), the situation became more complicated. One of the first unique discoveries of *ROSAT* was the observation of deep shadows in the general SXRB cast by the Draco Nebula ($l, b \sim 90°, 40°$, Burrows & Mendenhall 1991; Snowden et al. 1991). These observations unequivocally proved that there is significant $\frac{1}{4}$ keV X-ray emission in at least the lower Galactic halo: roughly 50% of the *observed* flux in that direction originates $\gtrsim$ 300 pc from the Sun, $\gtrsim$ 200 pc above the Galactic plane. Additional studies using both pointed observations and all-sky survey data demonstrated that the shadows were not unique to Draco but common features of the $\frac{1}{4}$ keV SXRB.

2   Data and Analysis

X-ray Data: This analysis uses the R1 and R2 band data (PSPC PI channels $8 - 19$ and $20 - 41$, respectively; Snowden et al. 1994) from the *ROSAT* all-sky survey (Snowden & Schmitt 1990) as presented in Snowden et al. (1997). The $\frac{1}{4}$ keV band is appropriate for the study of the LHB, as the LHB has a temperature near 10^6 K. Thermal equilibrium spectra near 10^6 K produce only $\sim$ 2% as many counts in the $\frac{3}{4}$ keV band as in $\frac{1}{4}$ keV band. The results of this analysis show that the temperature of much of the halo emission is near 10^6 K as well.

Measure of Galactic Absorption: Corrected *IRAS* 100 μm maps (Schlegel, Finkbeiner, & Davis 1997 and Finkbeiner, this volume) are used for Galactic absorption. The low spatial frequencies in the *IRAS* 100 μm data have been replaced by those from the well-calibrated *DIRBE* data. The *DIRBE* 100 μm, 140 μm, and 240 μm data have been used to determine temperature variations and to correct the 100 μm map to a constant reference temperature. In addition, the Leiden-Dwingeloo 21-cm survey data (Hartmann & Burton, 1997) in the velocity range from -74 km s^{-1} to 24 km s^{-1} in relatively low column density directions were used to determine a global normalization. Finally, the data were scaled to a column density of hydrogen.

In order to determine the foreground and distant (relative to the Galactic absorbing gas) contributions to the observed $\frac{1}{4}$ keV SXRB, the negative correlation (shadowing) between the $\frac{1}{4}$ keV background and the column density of absorbing material along the line of sight is examined. The sky is divided into $4°.8 \times 4°.8$ regions with $24' \times 24'$ pixels, and the negative correlation between X-ray intensity and H I column density as measured by the corrected

IRAS 100 μm data is fit for each band and region with a two-component absorption model. The spacing of the regions is $3°2 \times 3°2$, providing some angular overlap. The size of the region was minimized to sample as fine an angular structure as feasible and to reduce the effect of any intrinsic larger-scale variation. The region could not be made smaller without losing the needed dynamic range in the absorbing column density and affecting the robustness of the results. The overlap simply smooths the results.

The supposition is that on small angular scales no reasonable geometry will give a significant negative correlation due to displacement of H I by X-ray emitting gas, as clearly happens on large angular scales (e.g., SCMS). This is the critical difference between this work and previous studies. With the high angular resolution and statistical significance provided by the *ROSAT* data, the negative correlation of absorption on small angular scales can be distinguished from the presumed smoother, larger-scale variations of displacement.

With the X-ray intensity and effective N_{H} for each $24' \times 24'$ pixel, a two-component absorption model (foreground plus absorbed halo emission) plus a fixed extragalactic contribution, which is also absorbed,

$$I_X = I_0 + I_1 \times \exp[-\sigma(N_{\mathrm{H}}, T) \times N_{\mathrm{H}}] + I_{eg} \times \exp[-\sigma(N_{\mathrm{H}}, \alpha) \times N_{\mathrm{H}}],$$

was fit to all pixels in each $4°8 \times 4°8$ region independently for the R1 and R2 bands. I_X is the observed X-ray intensity, I_0 is the fitted foreground component, I_1 is the fitted halo component which is absorbed by the column density N_{H}, $\sigma(N_{\mathrm{H}}, T)$ is the theoretical band-averaged absorption cross section (Morrison & McCammon 1983) which is a function both of N_{H} and the temperature, T, of the thermal equilibrium emission model (Raymond & Smith 1977; Raymond 1991, see Snowden et al. 1994), I_{eg} is the fixed extragalactic contribution, and $\sigma(N_{\mathrm{H}}, \alpha)$ is the theoretical band-averaged absorption cross section which is a function both of N_{H} and power-law index, α. Temperature and emission measure results quoted here use the above thermal equilibrium emission models with solar abundances. The data were refit after the initial fitting produced an estimate of the halo temperature in order to use more appropriate absorption cross sections (a relatively insignificant effect).

I_{eg} was fixed using the results of recent observations of shadowing by extragalactic objects (a R1+R2 band flux of $\sim 400 \times 10^{-6}$ counts s^{-1} arcmin^{-2}, e.g., M101, Snowden & Pietsch 1995) and the extragalactic spectrum determined by Hasinger et al. (1993), $I(E) \sim E^{-1.96}$. The R2/R1 band ratio of 0.96 for the power law spectrum places 204×10^{-6} counts s^{-1} arcmin^{-2} in the R1 band and 196×10^{-6} counts s^{-1} arcmin^{-2} in the R2 band.

The existence of any additional emission in the region not considered by the model (e.g., if the region contains an SNR or cluster of galaxies) will increase the χ^2 statistic of the fit and affect the fitted parameters. Therefore, regions affected by a limited number of bright, small-scale extended sources such as the Cygnus Loop and Vela SNRs and the Virgo and Coma clusters of galaxies have been excluded. The existence of any clouds of sufficient column

density (e.g., $> 10^{19}$ cm^{-2}) floating in the LHB will also affect the results. However, since there is no indication of a large number of such clouds, this will only be to a limited extent and not affect the general analysis.

2.1   Foreground (LHB) Emission

Fitted and smoothed values for the foreground intensity (Fig. 1a) span a factor of ~ 3.3 from ~ 250 to $\sim 820 \times 10^{-6}$ counts s^{-1} arcmin^{-2}, implying emission measures of $0.0018 - 0.0058$ cm^{-6} pc. The general appearance is similar to that of the total background, with most of the same major features present but at only about half of the contrast: higher Galactic latitudes tend to have higher intensities and the lower intensities are near the Galactic plane. The largest region of highest intensity in the south is in the Galactic center hemisphere while in the north (other than Loop I) the major enhancements are mostly in the range $90° < l < 210°$.

Figure 2a shows a histogram of the R2/R1 band ratio (data from the atypical Loop I, Monogem, and Eridanus regions are excluded). The distribution is well peaked at a value of ~ 1.12 with half-maximum values of 1.02 and 1.23. These ratios can be interpreted as model emission temperatures of $10^{6.07}$ K, $10^{6.02}$ K, and $10^{6.12}$ K, respectively, assuming no foreground absorption. The R2/R1 band ratio over the sky for the LHB emission is relatively consistent with a single-temperature plasma.

2.2   Distant (Halo and Extragalactic) Emission

Assuming that the foreground emission, I_0, has been accurately determined, it is a simple matter to determine the magnitude and effective temperature of the distant component, $I_{dist} = I_{eg} + I_1$. Instead of using the fitted values for I_1, which have errors which are highly correlated with the errors of I_0 but are greater in magnitude, the smoothed I_0 map is used to evaluate the inverted equation:

$$I_{dist} = I_{eg} + I_1 = I_{eg} + (I_X - I_0 - I_{eg} \exp[-\sigma(N_{\mathrm{H}}, \alpha) \times N_{\mathrm{H}}])/$$

$$\exp[-\sigma(N_{\mathrm{H}}, T) \times N_{\mathrm{H}}].$$

In order to examine regions where the distant flux can be reasonably evaluated, only parts of the sky where $N_{\mathrm{H}} < 4.5 \times 10^{20}$ cm^{-2} were used. Figures 1b,c shows the results.

The distribution of the fitted R2/R1 band ratio in the polar regions differs slightly between north and south (see Fig. 2b, again excluding the regions contaminated by the Loop I, Monogem, and Eridanus enhancements). While both peak at R2/R1 ~ 1.01, the northern distribution is narrower than that in the south. Combining the two distributions, the half maxima are at 0.86 and 1.17 (temperatures of $10^{6.02}$ K, $10^{5.94}$ K, and $10^{6.10}$ K, respectively). The width of the curves and the fact that the extreme high-ratio wings lie outside

R1+R2 BAND I0 INTENSITY
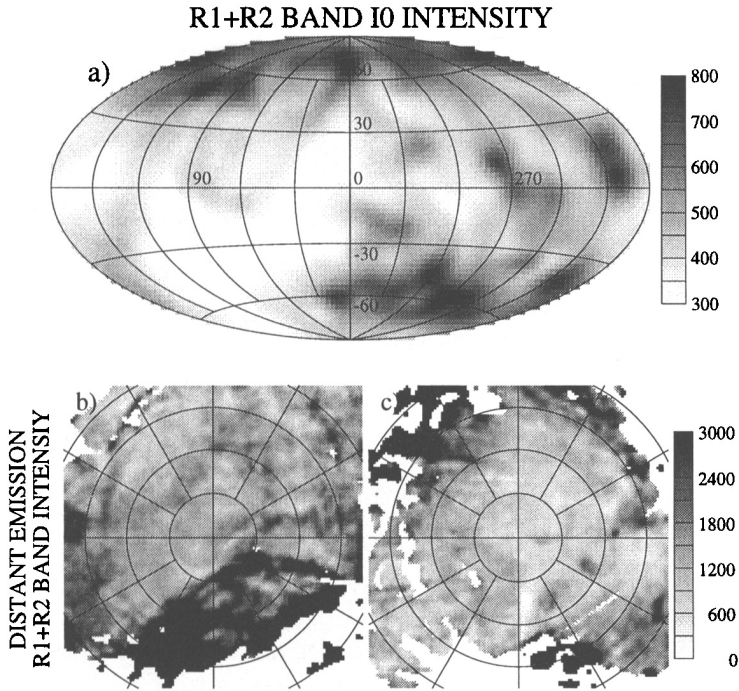
Fig. 1. a) Aitoff-Hammer projection in zero-centered Galactic coordinates of the I_0 fitted and smoothed intensity. b) North Galactic polar projection ($l = 0°$ is down, l increases clockwise) of the fitted and smoothed I_1 intensity. c) South Galactic polar projection ($l = 0°$ is up, l increases counterclockwise) of the fitted and smoothed I_1 intensity. Units are 10^{-6} counts s^{-1} arcmin^{-2}.
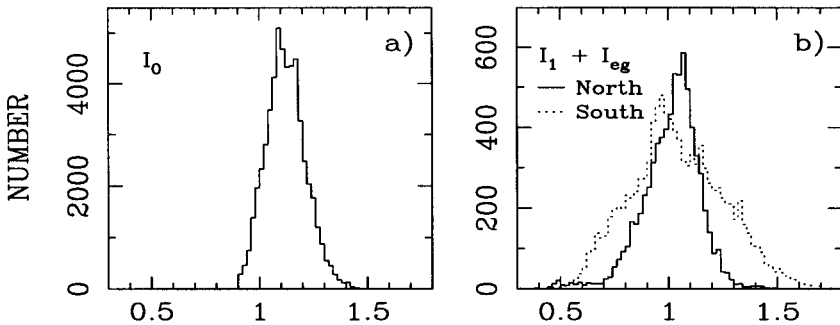
Fig. 2. Histograms of R2/R1 band ratios. a) Fitted foreground component, I_0. Typical uncertainties in the ratio are $\sim 0.05 - 0.1$. b) Fitted distant component, $I_{eg} + I_1$. typical uncertainties in the ratio are $\sim 0.1 - 0.2$. The solid line in b) shows the northern-hemisphere data while the dashed line shows the southern-hemisphere data. The vertical scaling is arbitrary as the plots oversample the data.

of the allowed model range (Snowden et al. 1994) can most likely be attributed to the uncertainties in the fitting procedure.

The unabsorbed $\frac{1}{4}$ keV band halo plus extragalactic intensities in the north away from Loop I have values ranging between ~ 400 and $\sim 3000 \times 10^{-6}$ counts s^{-1} arcmin^{-2}. Subtracting our assumed extragalactic contribution leaves a halo intensity of $\sim 0 - 2600 \times 10^{-6}$ counts s^{-1} arcmin^{-2}, emission measures of $\sim 0 - 0.017$ cm^{-6} pc.

The distant emission in the south is fairly flat near the pole with values between ~ 500 and $\sim 1200 \times 10^{-6}$ counts s^{-1} arcmin^{-2} (with at least some of the variation due to systematic uncertainties in the analysis). It increases with decreasing latitude from the pole up to intensities of a few thousand. This is qualitatively consistent with the latitude dependence of a plane-parallel distribution of the emitting material over the visible region of the halo, but is quantitatively too great an increase.

3   Discussion

3.1   The LHB and the $\frac{1}{4}$ keV SXRB

Although the LHB looks quite similar in appearance to the model of a decade ago (e.g., Cox & Reynolds 1987; SCMS), this similarity is in spite of the revolution in our understanding of the $\frac{1}{4}$ keV SXRB brought about by observations of significant diffuse X-ray emission in the Galactic halo.

Following the LHB model, the I_0 intensity map can be interpreted as a map of emission from the LHB, which in turn can be interpreted as a map of the radial extent of the LHB. The MBM12 shadowing results of Snowden, McCammon, & Verter (1993) can be used to fix a distance scale of 0.156 pc $(10^{-6}$ counts s^{-1} arcmin$^{-2})^{-1}$ to the radial extent of the LHB as a function of LHB emission. With this scale factor, the LHB extends from ~ 40 to ~ 130 pc depending on direction. Cuts of the LHB are shown in Figures 3. This is $\sim 30\%$ smaller than the less reliable minimum scaling of SCMS.

It must be noted, however, that the extent of the LHB is not necessarily the extent of the local cavity in the H I of the Galactic disk. In some directions, most notably in the direction of β CMa $(l, b = 226°, -14°, d = 203$ pc) in the third quadrant, the cavity extends $\gtrsim 200$ pc (e.g., Frisch & York 1983; Welsh et al. 1994) while the LHB, using the above scaling of the I_0 X-ray intensity, extends only to $\sim 60 - 95$ pc. The results of Gry, York, & Vidal-Madjar (1985) indicate that H II gas fills in at least some of the otherwise vacant line-of-sight. To further investigate this issue, the NaI ISM absorption line data of Welsh et al. (1994) have been used to compare the size of the cavity with the extent of the LHB. Figure 4 shows an Aitoff-Hammer projection of the positions of the Welsh et al. (1994) stars with different symbols depending on whether the data and model agree (plus signs, 54 stars, the stars have either 1) low column densities and distances and I_0 intensities which place
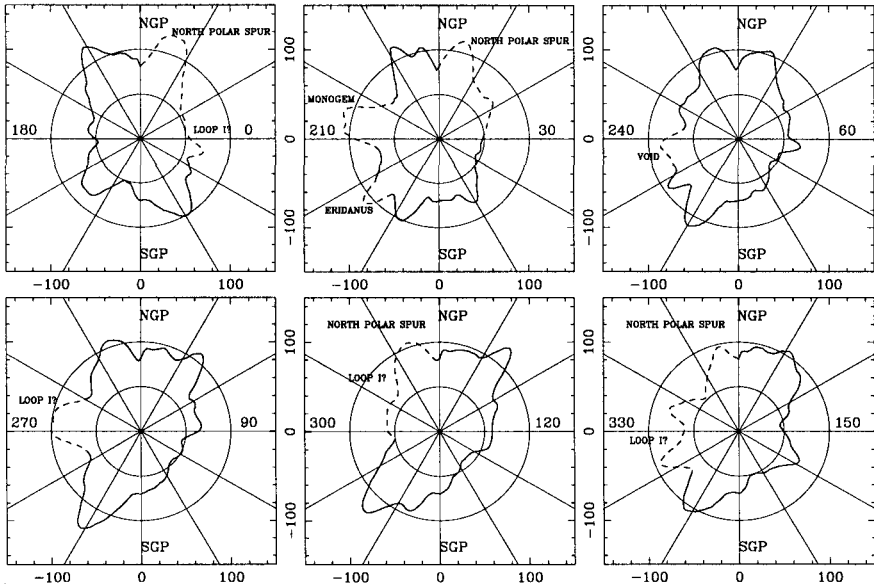
Fig. 3. Plots of the LHB radius in great-circle cuts through the Galactic poles along the labeled longitudes. The radii are derived from the fitted I_0 values: $R_{LHB} = 0.156 \times I_0$. The scale circles have radii of 50 pc and 100 pc. Regions which are contaminated by discrete features or are of other interest are labeled and the curves dashed.

them inside of the LHB or 2) high column densities and distances and I_0 intensities which place them outside of the LHB) or disagree (the stars have either 3) low column densities and distances and I_0 intensities which place them outside of the LHB or 4) high column densities and distances and I_0 intensities which place them inside of the LHB). Except for a limited number of stars (14, that appear relatively randomly distributed on the sky) which have foreground column densities placing them outside the cavity but $\frac{1}{4}$ keV I_0 intensities and distances placing them within the LHB (filled circles), the agreement appears reasonable. There are, however, a significantly greater number of stars (38) that the data imply are within the cavity but outside the LHB (open circles). About two-thirds of the latter group are found in two clusters, one centered near $(l, b \sim 340°, 0°)$ and the other centered near the third-quadrant void $(l, b \sim 240°, -15°)$, implying that the LHB may fill most if not all of the H I cavity in most other directions.

3.2 $\frac{1}{4}$ keV Emission in the Galactic Halo

Except for a limited number of regions such as Draco, the North Polar Spur, and southern latitudes with $b > -45°$, the halo emission of $\frac{1}{4}$ keV X-rays
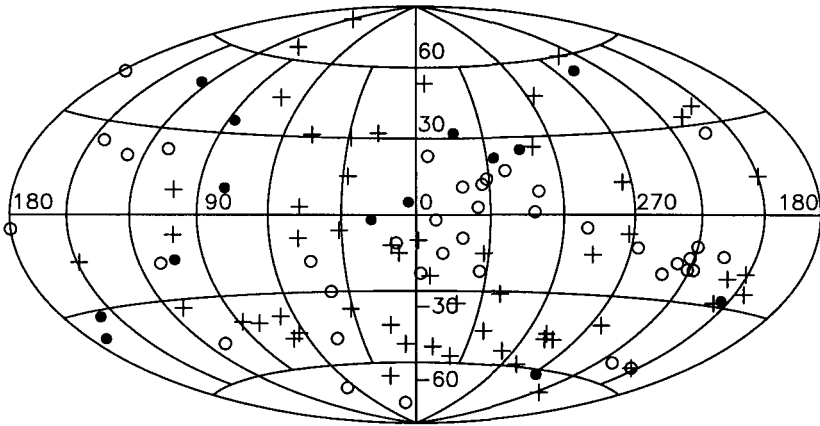
Fig. 4. Plot of the positions of the Welsh et al. (1994) stars in Galactic coordinates in an Aitoff-Hammer projection. Plus signs (+) indicate stars where the model agrees with the data, i.e., either the star has $< 5 \times 10^{18}$ cm^{-2} of foreground absorption and a distance which places it in the LHB or the star has $> 2 \times 10^{19}$ cm^{-2} of foreground absorption and a distance which places it outside of the LHB. Open circles indicate stars with distances placing them outside of the LHB but have foreground columns $< 5 \times 10^{18}$ cm^{-2}. Filled circles indicate stars with distances placing them inside of the LHB but have foreground columns $> 2 \times 10^{19}$ cm^{-2}. Errors in the stellar distances and measured column densities will obviously affect the plot.

varies over the range $\sim 200 - 1500 \times 10^{-6}$ counts s^{-1} arcmin^{-2} and is relatively isothermal (at least some of the temperature variation is likely due to limitations in the analysis technique and statistical errors). The Draco region, however, shows a strong intensity enhancement over a relatively limited solid angle (~ 0.03 sr). This enhancement, the first unambiguous Galactic halo emission discovered (Burrows & Mendenhall 1991; Snowden et al. 1991), has led to a biased view of the clumpiness of the halo emission as well as to an overestimate of the mean halo surface brightness.

The halo emission is brighter in the region of the north Galactic pole than the south while halo emission in the south increases more strongly toward lower latitudes. The longitude dependence at lower latitudes is considerably different in appearance between the northern and southern hemispheres as well, although this is dominated by distinct features such as the North Polar Spur in the north and Eridanus in the south.

The average values for the distant emission for latitudes $|b| > 65°$ are 1545×10^{-6} counts s^{-1} arcmin^{-2} for the north and 810×10^{-6} counts s^{-1} arcmin^{-2} for the south. After subtraction of the extragalactic contribution, they are reduced to 1145 and 410×10^{-6} counts s^{-1} arcmin^{-2}. The southern value lies well within the range of LHB emission while the northern value is only a factor of ~ 1.4 larger than peak LHB values.

The average values for the halo emission in the polar regions are roughly a factor of two lower than the $\frac{1}{4}$ keV surface brightness of the face-on spiral galaxy M101 at the equivalent position of the solar circle: $\sim 1570 \times 10^{-6}$ counts s^{-1} arcmin^{-2} (Snowden & Pietsch 1995). The sum of the average halo emission from $|b| > 65°$ corresponds to a luminosity of $\sim 6.6 \times 10^{36}$ ergs s^{-1} kpc^{-2}. Using values for Type I and Type II supernova rates and the average energy dumped into the interstellar medium by their explosions (and precursor winds for Type II) listed in Ferriére (1995), an average value of $\sim 8 \times 10^{38}$ ergs s^{-1} kpc^{-2} can be derived for near the solar circle. Thus the local halo emission at $\sim 10^6$ K constitutes $\sim 1\%$ of the average supernova power at the solar circle.

The surface brightness of the distant emission in a few regions both in the north and south is particularly low, $\lesssim 600 \times 10^{-6}$ counts s^{-1} arcmin^{-2}. If the presumed extragalactic background is subtracted, very little is left ($\lesssim 200 \times 10^{-6}$ counts s^{-1} arcmin^{-2}) that can be of halo origin, which again underscores the variation of the halo emission.

4   Conclusion

ROSAT all-sky survey data and *DIRBE*-corrected *IRAS* 100 μm data have been used to study the distribution of emission responsible for the observed $\frac{1}{4}$ keV diffuse background. Emission from the Local Hot Bubble dominates the background at low Galactic latitudes and contributes much of the observed flux at high latitudes as well. The emission temperature of the LHB is in the range $10^{6.07 \pm 0.05}$ K and the intensity varies between ~ 250 and 820×10^{-6} counts s^{-1} arcmin^{-2}. The intensity of the LHB emission can be used to estimate its radial extent from the Sun, which varies between 40 pc and 130 pc. Since the intensities are generally greater at higher Galactic latitudes, they are strongly anticorrelated with total H I column density, presumably due to displacement effects as discussed in Sanders et al. (1977), McCammon & Sanders (1990), and SCMS. The LHB extends further toward the Galactic poles than in the plane, although the regions of greatest extent are not at the poles themselves. No strong enhancement is found in the direction of the third-quadrant void, implying that it is not filled with 10^6 K plasma in thermal pressure equilibrium with the LHB.

Consistent with previous shadowing studies, extensive $\frac{1}{4}$ keV emission is found in the Galactic halo with emission temperatures in the range $10^{6.02 \pm 0.08}$ K and the derived intensity outside the absorbing layer varies from near zero to $> 3000 \times 10^{-6}$ counts s^{-1} arcmin^{-2} in some regions at lower Galactic latitude. Also consistent with previous studies, the halo emission can vary by a factor of two over angular scales of $\sim 20°$. The average halo unabsorbed intensity in the south polar region is $\sim 410 \times 10^{-6}$ counts s^{-1} arcmin^{-2}, which is comparable to typical values for the LHB emission. The average value for the north polar region is $\sim 1140 \times 10^{-6}$ counts s^{-1} arcmin^{-2}, which is about

1.4 times the peak values for the LHB emission. Thus while there are some halo regions which are a factor of four or so brighter than the brightest LHB regions (e.g., Draco), more typical high-latitude values are similar to those in the LHB.

References

Bowyer, C. S., Field, G. B., & Mack, J. E. 1968, Nature, 217, 32

Burrows, D. N. 1989, ApJ, 340, 775

Burrows, D. N., Kraushaar, W. L., McCammon, D., & Sanders, W. T. 1984, ApJ, 287, 208

Burrows, D. N., & Mendenhall, J. A. 1991, Nature, 351, 629

Cox, D. P., & Reynolds, R. J. 1987, ARA&A, 25, 303

Ferriére, K. M. 1995, ApJ, 441, 281

Frisch, P. C., & York, D. G. 1983, ApJL, 271, L59

Gry, C., York, D. G., & Vidal-Madjar, A. 1985, ApJ, 296, 593

Hasinger, G., et al. 1993, A&A, 275, 1

Hartman, D. & Burton, W. B. 1997, Atlas of Galactic Neutral Hydrogen, (Cambridge University Press:Cambridge)

Jakobsen, P., & Kahn, S. M. 1986, ApJ, 309, 682

Knapp, G. R. 1975, AJ, 80, 111

Marshall, F. J., & Clark, G. W. 1984, ApJ, 287, 633

McKee, C. F., & Ostriker, J. P. 1977, ApJ, 218, 148

Morrison, R., & McCammon, D. 1983, ApJ, 270, 119

Raymond, J. C. 1991, private communication, computer code update

Raymond, J. C., & Smith, B. W. 1977, ApJS, 35, 419

Sanders, W. T., Kraushaar, W. L., Nousek, J. A., & Fried, P. M. 1977, ApJL, 217, L87

Schlegel, D. J., Finkbeiner, D. P., Davis, M. 1997, in preparation

Snowden, S. L., Cox, D. P., McCammon, D., & Sanders, W. T. 1990, ApJ, 354, 211, SCMS

Snowden S.L., Egger R., Freyberg M.J., McCammon D., Plucinsky P.P., Sanders W.T., Schmitt J.H.M.M., Trümper J., Voges W., 1997, ApJ, 485, 125

Snowden, S. L., McCammon, D., Burrows, D. N., & Mendenhall, J. A. 1994, ApJ, 424, 714

Snowden, S. L., McCammon, D., & Verter, F. 1993, ApJL, 409, L21

Snowden, S. L., Mebold, U., Hirth, W., Herbstmeier, U., & Schmitt, J. H. M. M. 1991, Science, 252, 1529

Snowden, S. L., & Pietsch, W. 1995, ApJ, 452, 627

Snowden, S. L., & Schmitt, J. H. M. M. 1990, Ap&SS, 171, 207

Trümper, J. 1983, Adv. Space Res., 2(4), 241

Welsh, B. Y., Craig, N., Vedder, P. W., & Vallerga, J. V. 1994, ApJ, 437, 638